

A novel high breakdown voltage and high switching speed GaN HEMT with p-GaN gate and hybrid AlGaN buffer layer for power electronics applications

Yong Liu(刘勇), Qi Yu(于奇), and Jiang-Feng Du(杜江锋)
Citation: Chin. Phys. B, 2020, 29 (**12**): 127701. DOI: 10.1088/1674-1056/abae
Journal homepage: http://cpb.iphy.ac.cn; http://iopscience.iop.org/cpb

What follows is a list of articles you may be interested in

Surface termination effects on the electrical characteristics of La_2O_3/Al_2O_3 nanolaminates deposited by atomic layer deposition

Ji-Bin Fan(樊继斌), Shan-Ya Ling(凌山雅), Hong-Xia Liu(刘红侠), Li Duan(段理), Yan Zhang(张研), Ting-Ting Guo(郭婷婷), Xing Wei(魏星), and Qing He(何清)
Chin. Phys. B, 2020, 29 (**11**): 117701. DOI: 10.1088/1674-1056/abc0d4

Variable-*K* double trenches SOI LDMOS with high-concentration P-pillar

Lijuan Wu(吴丽娟), Lin Zhu(朱琳), Xing Chen(陈星)
Chin. Phys. B, 2020, 29 (**5**): 057701. DOI: 10.1088/1674-1056/ab7e94

Improvement of the high-κ/Ge interface thermal stability using an *in-situ* ozone treatment characterized by conductive atomic force microscopy

Ji-Bin Fan(樊继斌), Xiao-Jiao Cheng(程晓姣), Hong-Xia Liu(刘红侠), Shu-Long Wang(王树龙), Li Duan(段理)
Chin. Phys. B, 2017, 26 (**8**): 087701. DOI: 10.1088/1674-1056/26/8/087701

A novel P-channel SOI LDMOS structure with non-depletion potential-clamped layer

Wei Li(李威), Zhi Zheng(郑直), Zhigang Wang(汪志刚), Ping Li(李平), Xiaojun Fu(付晓君), Zhengrong He(何峥嵘), Fan Liu(刘凡), Feng Yang(杨丰), Fan Xiang(向凡), Luncai Liu(刘伦才)
Chin. Phys. B, 2017, 26 (**1**): 017701. DOI: 10.1088/1674-1056/26/1/017701

Non-depletion floating layer in SOI LDMOS for enhancing breakdown voltage and eliminating back-gate bias effect

Zheng Zhi, Li Wei, Li Ping
Chin. Phys. B, 2013, 22 (**4**): 047701. DOI: 10.1088/1674-1056/22/4/047701

A novel high breakdown voltage and high switching speed GaN HEMT with p-GaN gate and hybrid AlGaN buffer layer for power electronics applications*

Yong Liu(刘勇), Qi Yu(于奇), and Jiang-Feng Du(杜江锋)†

State Key Laboratory of Electronic Thin Films and Integrated Devices, School of Electronic Science and Engineering, University of Electronic Science and Technology of China, Chengdu 610054, *China*

(Received 11 June 2020; revised manuscript received 21 July 2020; accepted manuscript online 13 August 2020)

A novel p-GaN gate GaN high-electron-mobility transistor (HEMT) with an AlGaN buffer layer and hybrid dielectric zone (H-HEMT) is proposed. The hybrid dielectric zone is located in the buffer and composed of horizontal arranged HfO_2 zone and SiN_x zone. The proposed H-HEMT is numerically simulated and optimized by the Silvaco TCAD tools (ATLAS), and the DC, breakdown, *C*–*V* and switching properties of the proposed device are characterized. The breakdown voltage of the proposed HEMT is significantly improved with the introduction of the hybrid dielectric zone, which can effectively modulate the electric field distribution in the GaN channel and the buffer. High breakdown voltage of 1490 V, low specific on-state resistance of 0.45 mΩ·cm^2 and high Baliga's figure of merit (FOM) of 5.3 GW/cm^2, small $R_{on}Q_{oss}$ of 212 mΩ·nC, high turn-on speed 627 V/ns and high turn-off speed 87 V/ns are obtained at the same time with the gate-to-drain distance L_{gd} of 6 μm.

Keywords: GaN HEMT, breakdown voltage, high-permittivity dielectric, low-permittivity dielectric

PACS: 73.40.Kp, 73.61.Ey, 78.30.Fs, 77.22.Ch **DOI:** 10.1088/1674-1056/abaee5

1. Introduction

Gallium nitride (GaN) high electron mobility transistors (HEMTs) based on AlGaN/GaN heterojunctions have attracted a great deal of attention recently owing to their better characteristics, i.e., high mobility, high-electron saturation velocity, and high breakdown voltage (BV).[1–5] For power electronics applications, GaN HEMTs are more attractive compared with silicon-based power devices because of their higher critical breakdown electric field and higher current driving capability.[6,7] For safe-failed operation and simple drive circuits, designs of normally-off GaN devices are essential,[8,9] and several techniques to realize normally-off GaN devices have been proposed like thin AlGaN barrier,[10] fluorine implantation,[11] trench gate.[12] Recently p-GaN gate technique has become the most prevalent method to achieve normally-off GaN HEMTs,[13–15] and based on this technique several high breakdown voltage GaN HEMTs with high breakdown voltage and high switching speed have been released.[16,17] As far as we know for p-GaN gate GaN HEMTs the highest average breakdown electric field and figure of merit (FOM) are 1.4 MV/cm and 3.9 GW/cm^2.[16] The highest turn-on speed (dV_{ds}/dt) for GaN power devices as we know is 267 V/ns (with t_r of 1.2 ns),[18] and the highest turn-off speed for GaN power devices as we know is 285 V/ns (with t_f of 1.12 ns).[16]

Although many efforts have been taken to p-GaN gate GaN HEMTs to obtain high breakdown voltage and high switching speed, there is still huge space to promote GaN HEMTs' breakdown and switching performances. Indeed similar with conventional normally-on GaN HEMTs, under off-state breakdown conditions p-GaN gate GaN HEMTs also face the problem of electric field crowding at the drain electrode or gate electrode. One usual method to admire the electric field crowding is field plate technique,[2] however it could introduce an additional parasitic capacitance and could result in the degradation of the switching performances of the devices. Another usual method to solve the problem of electric field crowding is AlGaN back barrier technique,[19] however the average breakdown electric field strength is still far from reaching the GaN's critical breakdown electric field (3 MV/cm).

To improve GaN HEMTs' breakdown voltages and switching speeds a novel GaN HEMT with p-GaN gate, AlGaN buffer and high-*k*/low-*k* hybrid dielectric zone structure is proposed, simulated and optimized. Owing to the difference of relative permittivity of HfO_2 and SiN_x the hybrid dielectric zone structure could modulate the electric field distribution in the channel to be more uniform under breakdown conditions, thus the BV of the proposed H-HEMT can be significantly promoted. In addition, the back barrier produced by the AlGaN buffer can also improve the confinement of the two-dimensional electronic gas (2-DEG) and modulate the electric field distribution, which can further improve the breakdown voltage and switching speed. The numeric simulation of the proposed device is conducted using the Silvaco tools (AT-

*Project supported by the National Natural Science Foundation of China (Grant No. 61376078).

†Corresponding author. E-mail: jfdu@uestc.edu.cn

© 2020 Chinese Physical Society and IOP Publishing Ltd

LAS), and during the simulation the polarization model, low field mobility model, high field mobility model and Selberherr's impact ionization model are comprehensively considered. To obtain the switching performances of the proposed device a hybrid simulation based on Silvaco tools is also established. For comparison, a GaN HEMT with p-GaN gate and GaN buffer (Conv HEMT) and a GaN HEMT with p-GaN gate and AlGaN buffer (A-HEMT) are also simulated and analyzed. With proper design and optimization the proposed H-HEMT possesses low $R_{on,sp}$, high breakdown voltage, high Baliga's figure of merit (FOM) and high switching speed at the same time, demonstrating a great prospect in power electronics applications.

2. Device structure and simulations

2.1. Device structure and fabrication process

Figure 1 shows the device structures of the conventional p-GaN gate GaN HEMT (Conv HEMT) with GaN buffer (Fig. 1(a)), the p-GaN gate GaN HEMT (A-HEMT) with $Al_{0.25}Ga_{0.75}N$ buffer (Fig. 1(b)), and the proposed p-GaN gate GaN HEMT (H-HEMT) with $Al_{0.25}Ga_{0.75}N$ buffer and hybrid dielectric zone (Fig. 1(c)). For the proposed H-HEMT the buffer is composed of the $Al_{0.25}Ga_{0.75}N$, HfO_2 zone and SiN_x zone, and the interface of HfO_2/SiN_x is set between gate and drain. The width of HfO_2 zone and SiN_x zone are set as 1 μm and 1.5 μm, respectively. For all the three kinds of devices in this study the Al composition of the AlGaN barrier, doping concentration of the p-GaN layer, and the gate width were all set as 0.26, 3×10^{17} cm^{-3} and 1 mm, respectively. Other main structural parameters of the three devices are set as the same and their ranges are listed in Table 1. For the proposed H-HEMT the location of the HfO_2/SiN_x interface (L_{gi}), distance between the hybrid dielectric zone and GaN channel (T_{ci}), gate-to-drain distance L_{gd} have been optimized.

Table 1. Main parameters of the proposed GaN HEMTs.

Parameters	Units	Values	Parameter captions
L_s	μm	1	Length of source electrode
L_g	μm	1	Length of gate electrode
L_d	μm	1	Length of drain electrode
L_{gi}	μm	1–5	Gate-to-interface distance
L_{gs}	μm	1	Gate-to-source distance
L_{gd}	μm	5–20	Gate-to-drain distance
T_{p-GaN}	nm	110	Thickness of p-GaN layer
T_{bar}	nm	15	Thickness of AlGaN barrier
T_{ch}	nm	85	Thickness of GaN channel
T_{buff}	μm	2	Thickness of buffer layer
T_{ci}	μm	0–2	Al composition of $Al_aGa_{1-a}N$

The fabrication process of the proposed H-HEMT can be the same as that of the reported p-GaN gate GaN HEMT with AlGaN buffer.[20] The p-GaN/AlGaN/AlGaN heterostructures are grown by MOCVD on Si substrates. Ohmic source and drain contacts are defined and metalized after selectively plasma-etching a p-GaN cap layer, except for the gates. The devices can be isolated by nitrogen implantation and can be passivated with plasma-enhanced chemical vapor deposition (PECVD) SiN_x. Then the Si substrate beneath the high-k/low-k hybrid dielectric zone is removed by SF_6 plasma etching to make the AlGaN buffer exposed. A partial AlGaN buffer is removed by BCl_3/Cl_2 gas plasma to the designed location. Then PECVD SiN_x would fill the etched AlGaN zone and be partially etched as design, after which the high-k dielectric HfO_2 is deposited in the etched SiN_x zone.

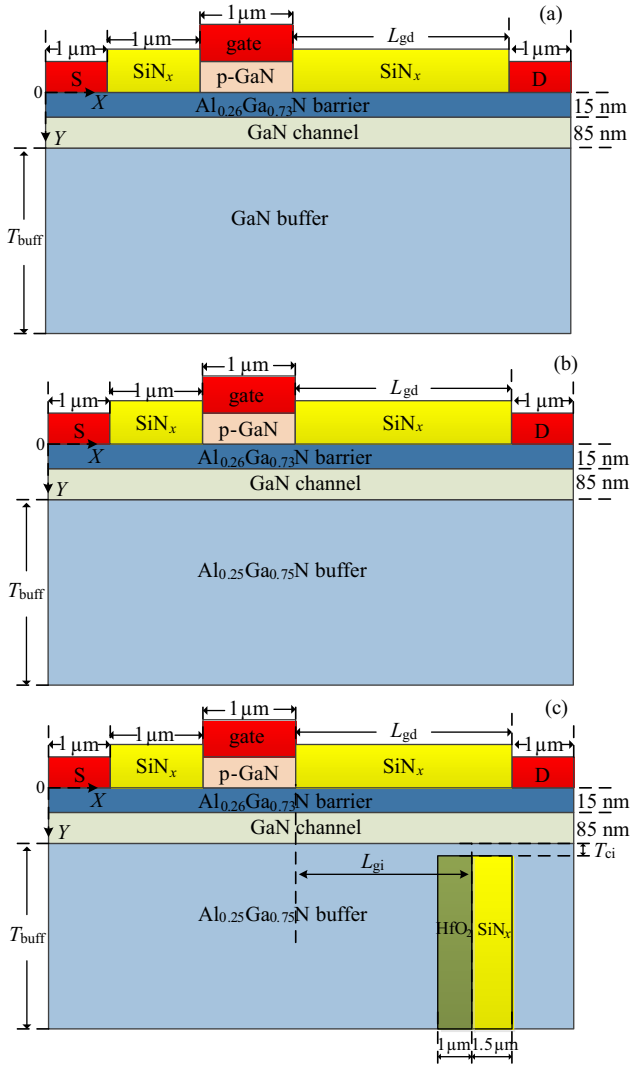


Fig. 1. Schematic figures of the Conv HEMT (a), A-HEMT (b) and the proposed H-HEMT (c). S: source, D: drain.

2.2. Simulation models and calibration

The proposed devices have been simulated and optimized using Silvaco TCAD tools (ATLAS), and during the simulations the Shockley–Read–Hall model (SRH), Fermi–Dirac model, polarization model, low field mobility model, high field mobility model (velocity saturation mobility model) and Selberherr's impact ionization model are adopted. In the unintentional doped GaN buffer or AlGaN buffer ac-

ceptor trap with energy level of $E_c = 0.5$ eV and concentration of 1×10^{17} cm^{-3} is inserted.[21] A normally-on GaN HEMT fabricated and measured by us[22] is used to calibrate the simulations for the proposed devices. The normally-on GaN HEMT is composed of Si substrate, 3-μm-thick GaN buffer layer, 100-nm-thick GaN channel layer, and 15-nm-thick $Al_{0.23}Ga_{0.77}N$ barrier layer, 20-nm-thick LPCVD SiN_x as gate insulator, source electrode, drain electrode, gate electrode and 150-nm-thick PECVD SiN_x as surface passivation layer. For the fabricated normally-on GaN HEMT the gate width (W_g), gate length (L_g), gate-to-source distance L_{gs} and the gate-to-drain distance L_{gd} are 250 μm, 2 μm, 2 μm, and 2 μm, respectively. The normally-on GaN HEMT has been fabricated using the regular GaN fabrication process including mesa isolation, source and drain electrode deposition (Ti/Al/Ni/Au), gate insulator deposition (LPCVD SiN_x), gate electrode deposition (Ni/Au) and surface passivation (PECVD SiN_x). The normally-on GaN HEMT has been simulated using the Silvaco ATLAS tools and the models discussed above are adopted to calibrate the simulation model and parameters. The simulated normally-on GaN HEMT has a threshold voltage of −7.8 V, which is consistent with the experimental results.[22] The output characteristics of the measured and simulated results for the GaN HEMT are shown in Fig. 2. The simulated results show great fitting accuracy compared with the measured results, demonstrating the good accuracy of the simulation models we used for GaN HEMTs.

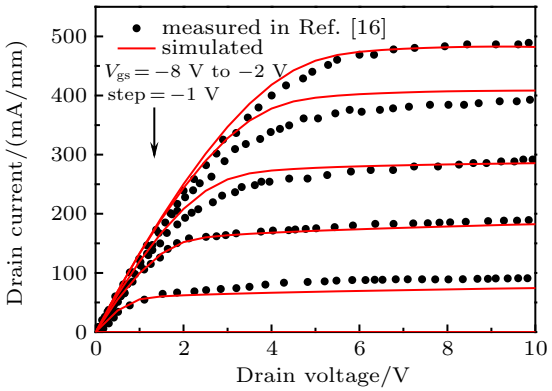


Fig. 2. Experimental and simulated output characteristics for the normally-on GaN HEMT after calibrating the simulation models.

2.3. Device-circuit hybrid simulation for switching properties

To characterize the switching performances of the proposed device, a device-circuit hybrid simulation system based on Silvaco has been established. The hybrid simulation system is composed of two parts, i.e., static part and dynamic part. The simulation is firstly conducted with the static part to get the initial static results, and then the initial static results are loaded in the dynamic part as preliminary solutions. The circuit used for the switching simulation is shown in Fig. 3, in which the 0.2 mH inductance acts as the load and the diode acts as the freewheeling diode. During the simulation the static part is obtained when the device is biased by 0 V gate voltage and 400 V drain voltage. In the transient part the gate driver signal is a voltage pulse signal with period of 1 μs (1 MHz and duty ratio of 50%). In the simulation, t_r and t_f are defined as the times for V_{ds} to climb from 10% to 90% and decline from 90% to 10%, respectively.

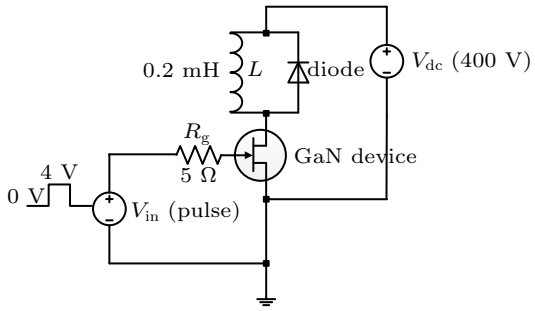


Fig. 3. Schematic figure of the electric circuit used for the hybrid simulation for switching performances of the GaN HEMT devices.

3. Results and discussion

3.1. DC properties

Figure 4(a) shows the simulated electron concentration distributions in different zones for the Conv HEMT, A-HEMT, H-HEMT ($T_{ci} = 0$) and H-HEMT ($T_{ci} = 50$ nm) under zero bias ($V_{ds} = 0$ V, $V_{gs} = 0$ V). The A-HEMT and proposed H-HEMT with AlGaN buffer or hybrid AlGaN buffer have better confinement for 2-DEG in the GaN channels. The H-HEMT ($T_{ci} = 50$ nm) has better 2-DEG confinement than the H-HEMT ($T_{ci} = 0$), because for the H-HEMT ($T_{ci} = 0$) the AlGaN back barrier between GaN channel and the high-k/low-k hybrid dielectric zone is gone. Figure 4(b) shows the extracted electron concentration distributions along the GaN channel, where Y is fixed at 15 nm. The A-HEMT and H-HEMTs have slightly lower electron concentration in the GaN channel than that of the Conv HEMT, which would make them to undertake higher off-state drain voltage with slight sacrifice of output current.

The simulated transfer and output properties of the Conv HEMT, the A-HEMT and the proposed H-HEMT devices are shown in Figs. 5(a) and 5(b), respectively. For the Conv HEMT, the threshold voltage V_{th} is 1 V, which is consistent with the reported results of the p-GaN gate GaN HEMT.[17] Owing to the $Al_{0.25}Ga_{0.75}N$ back barrier the V_{th} values of the A-HEMT, H-HEMT ($T_{ci} = 0$) and H-HEMT ($T_{ci} = 50$ nm) V_{th} are increased to 1.8 V compared with the Conv-HEMT. For the Conv-HEMT, the A-HEMT, H-HEMT ($T_{ci} = 0$) and H-HEMT ($T_{ci} = 50$ nm), the saturation current densities at $V_{gs} = 3$ V are 0.62 A/mm, 0.43 A/mm, 0.41 A/mm and 0.41 A/mm, respectively. Extracted from Fig. 5(b) the specific on-state resistance ($R_{on,sp}$) of the Conv-HEMT, the A-HEMT, H-HEMT ($T_{ci} = 0$) and H-HEMT ($T_{ci} = 50$ nm) are

identified as 0.4 mΩ·cm^2, 0.45 mΩ·cm^2, 0.45 mΩ·cm^2 and 0.45 mΩ·cm^2. Compared with the Conv-HEMT the $R_{on,sp}$ is slightly increased for the proposed H-HEMT. However, the $R_{on,sp}$ for the proposed H-HEMT is still lower than that of the reported GaN HEMTs.[23,24]

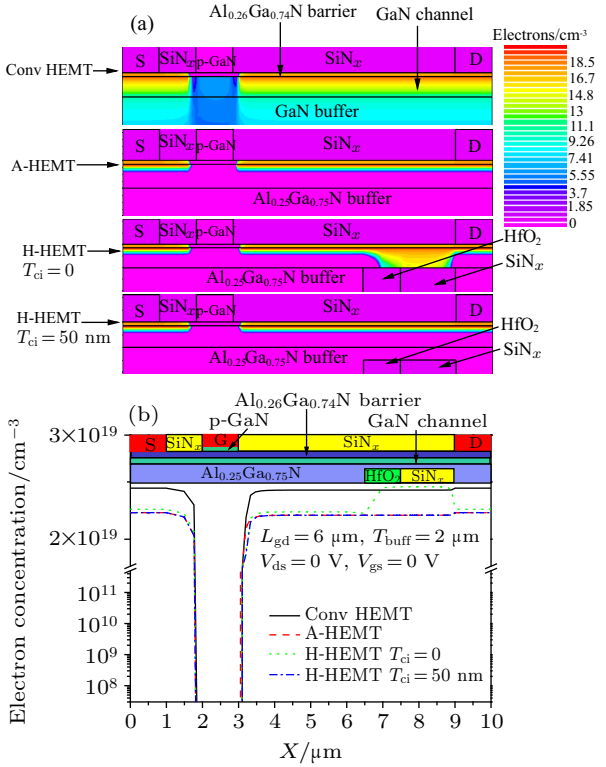


Fig. 4. Electron concentration distributions in the whole device (a) and along the GaN channel where $Y = 15$ nm for the HEMT devices (b).

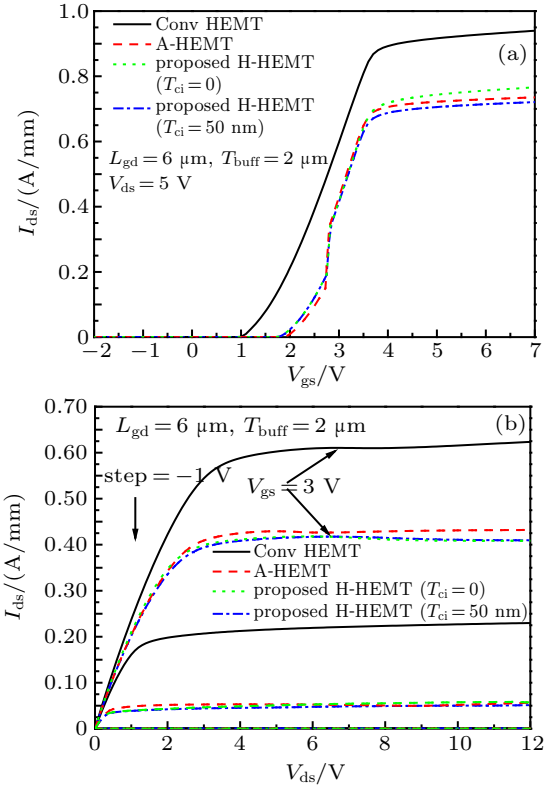


Fig. 5. Transfer properties (a) and output properties (b) of the GaN HEMT devices.

3.2. Breakdown properties

During the breakdown simulation the gate is biased by a −3 V voltage to shut down the devices, and the off-state breakdown voltage is defined as the drain voltage V_{ds}@I_{ds} = 1 μA/mm. Figure 6 shows the electric field distributions between gate and drain for the GaN HEMT devices under breakdown conditions. For the Conv HEMT the electric field in the buffer is concentrated near the gate electrode (about 2.4 MV/cm), and the electric field in the other buffer zone is as low as 0.4 MV/cm. For the A-HEMT the electric field in the middle of the buffer was elevated to be about 1.4 MV/cm. For the proposed H-HEMT the electric field in the HfO_2 zone is higher than the electric field in the SiN_x zone. According to Gauss's law the horizontal electric fields in the HfO_2 zone E_1 and in SiN_x zone E_2 have a relationship as follows:

$$\varepsilon_1 E_1 = \varepsilon_2 E_2, \tag{1}$$

where ε_1 and ε_2 are the relative permittivity for HfO_2 and SiN_x, respectively. Due to the difference between ε_1 and ε_2, there is a discontinuity of the horizontal electrical field at the HfO_2/SiN_x interface, which can be seen in Fig. 6. The high electric field in the SiN_x zone would elevate the electric field in the GaN channel above the SiN_x zone, thus the electric field in the GaN channel could be modulated to be more uniform which could improve the BV of the H-HEMT.

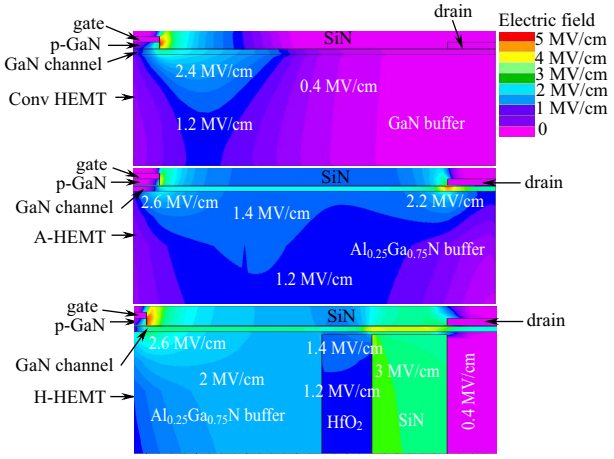


Fig. 6. Electric field distributions between gate and drain for GaN HEMT devices under breakdown conditions.

Figure 7(a) shows the electric field distributions along the GaN channels extracted from Fig. 6 under breakdown conditions for GaN HEMT devices with different buffer structures. It can be seen that for the Conv HEMT and the A-HEMT the electric field crowding phenomenon is observed. For the Conv HEMT the electric field crowding is near the gate edge, but for the A-HEMT the electric field peak near the gate edge is weakened and another higher electric field peak is generated at the drain edge similar with the experimental results.[17] As shown in Fig. 7(a) for the proposed H-HEMT the HfO_2/SiN_x structure could introduce an electric field peak in the GaN channel

above the $Al_aGa_{1-a}N/Al_bGa_{1-b}N$ interface, and the electric field distribution along the channel becomes more uniform. Figure 7(b) shows the simulated off-state breakdown curves of the GaN HEMTs with different buffer structures. Simulated breakdown voltage (BV) for the Conv HEMT, the A-HEMT and the proposed H-HEMT is identified as 500 V, 817 V and 1490 V, respectively. Compared with the Conv HEMT and the A-HEMT devices the proposed H-HEMT shows higher breakdown voltage and maintains a relative small $R_{on,sp}$, demonstrating its great superiority for power electronics applications.

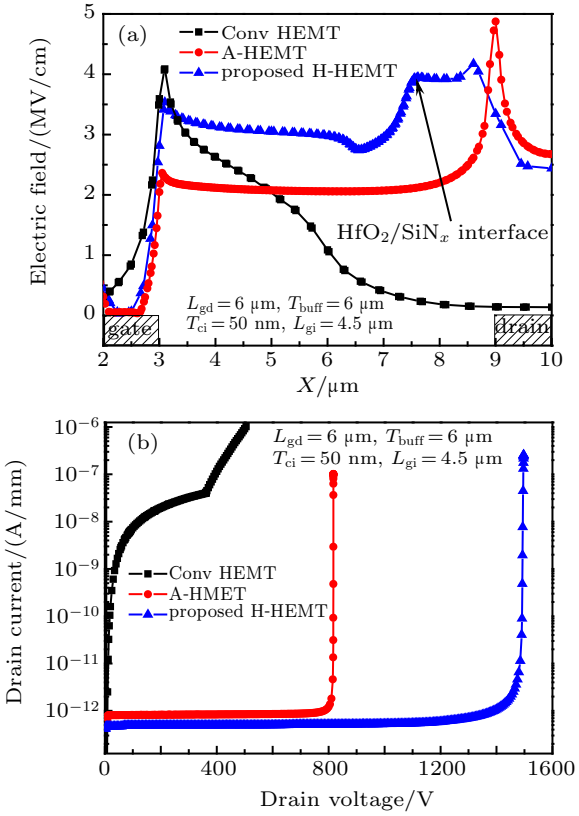


Fig. 7. Simulated breakdown curves (a) and electric field distributions along the GaN channels (b) for GaN HEMT devices under breakdown conditions.

Breakdown voltages for the proposed H-HEMT with different locations of the HfO_2/SiN_x interface have been simulated to obtain the optimal value of L_{gi}. Figure 8(a) shows the electric field distributions along the GaN channels for the proposed H-HEMT devices with different L_{gi} under breakdown conditions. When L_{gi} is smaller than 4.5 μm the electric field peak near the gate is weakened compared with the Conv HEMT (Fig. 8(a)), and the electric field peak near the drain is also weakened compared with the A-HEMT (Fig. 8(a)). When L_{gi} is 5 μm the electric field distributions along the GaN channel is similar to that for the A-HEMT, and the influence of the hybrid dielectric zone on the electric field distributions can be neglected. The most uniform electric field distributions for the GaN channel are obtained when L_{gi} is 4.5 μm, for which the electric field crowding near the gate and drain are not significant and the electric field between the gate and drain is close to be flat. Figure 8(b) shows that the highest BV (1490 V) is obtained for the proposed H-HEMT with L_{gi} of 4.5 μm, thus the optimal value of L_{gi} for the proposed H-HEMT with L_{gd} of 6 μm is identified as 4.5 μm.

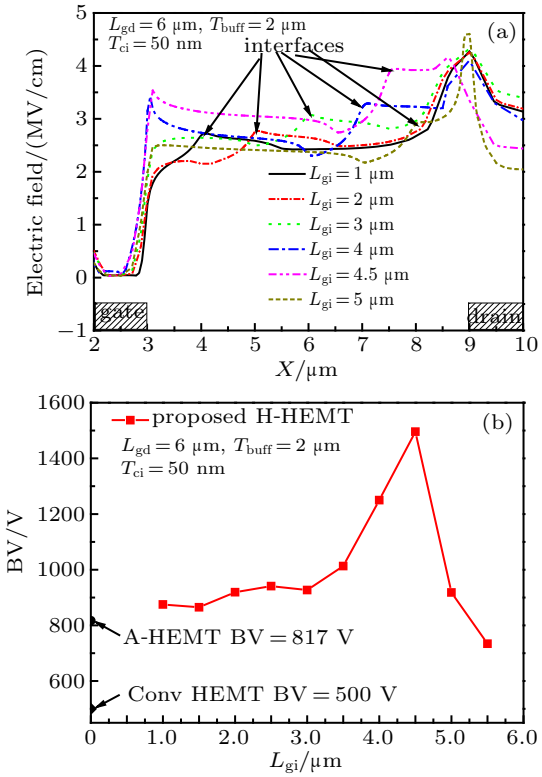


Fig. 8. Electric field distributions along GaN channels (a) and BV of the proposed H-HEMT devices (b) versus L_{gi}.

The distance between the top surfaces of the hybrid dielectric zone and the bottom of the GaN channel has also been optimized to obtain higher BV. As shown in Fig. 9(a) with given values of L_{gi}, the electric field strength near the gate is decreased with the increase of T_{ci}. The electric field strength near the drain is increased with the increase of T_{ci}, which means that the modulation of the electric field would be weakened with large T_{ci}. When T_{ci} is 0 the hybrid dielectric zone surfaces are contacted with the bottom of the GaN channel, for which the AlGaN back barrier between the GaN channel and the hybrid dielectric zone is gone. The electric field peak is transferred from the drain edge to the HfO_2/SiN_x interface when T_{ci} is 0, thus it is better for the T_{ci} to be larger than 0. Figure 9(b) shows the simulated BV for the proposed H-HEMT devices with different T_{ci}. It can be seen that the highest BV (1490 V) is obtained with T_{ci} of 50 nm. Therefore the optimal value of T_{ci} is identified as 50 nm considering the breakdown properties.

For the proposed H-HEMT when the gate-to-drain distance L_{gd} is increased the optimal value of L_{gi} is also increased, and the optimal L_{gi} for the H-HEMT with different L_{gd} has

also been simulated and identified as $L_{gi} = L_{gd} - 1.5$ μm. Figure 10 shows the simulated BV, $R_{on,sp}$ and calculated FOM for the proposed H-HEMT devices versus L_{gd}, where the L_{gi} is set as the optimal value and T_{ci} is set as 50 nm. It can be seen that the breakdown voltage of the proposed H-HEMT increases linearly with the increase of L_{gd}, and when L_{gd} is increased from 5 μm to 20 μm the BV is increased from 1200 V to 3600 V. The trade-off between BV and $R_{on,sp}$ is usually characterized by the figure-of-merit (FOM) of $BV^2/R_{on,sp}$, and the FOMs for the proposed H-HEMT devices with different L_{gd} have been calculated as shown in Fig. 10. The value of FOM maintains higher than 4 GW/cm^2 when L_{gd} increases from 5 μm to 20 μm, and the FOM is as high as 5.3 GW/cm^2 for the proposed H-HEMT with L_{gd} of 6 μm.

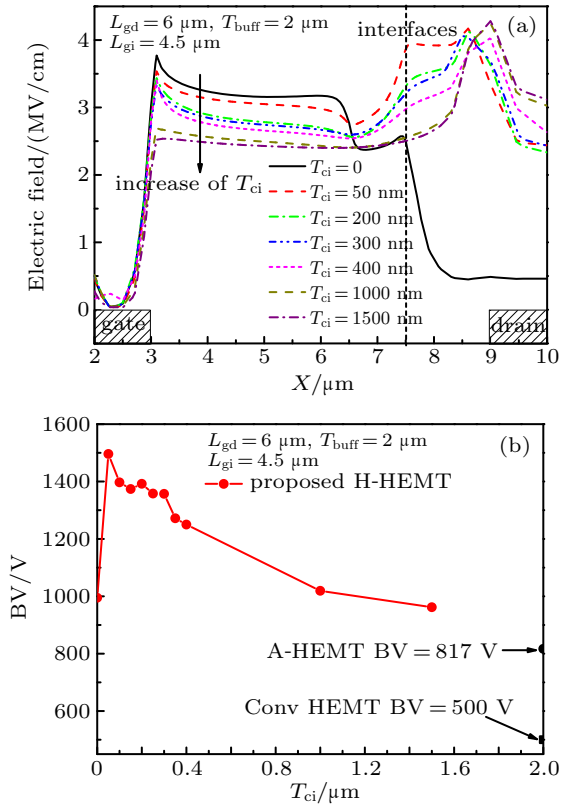


Fig. 9. Electric field distributions along the GaN channels (a) and breakdown voltages (b) for the proposed H-HEMT devices versus T_{ci}.

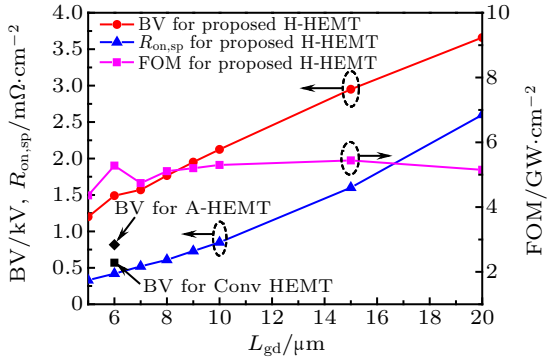


Fig. 10. Simulated breakdown voltages, $R_{on,sp}$ and FOM ($BV^2/R_{on,sp}$) versus L_{gd} for the proposed H-HEMT devices.

Figure 11 shows the benchmark plot of BV versus $R_{on,sp}$ for the Conv HEMT, A-HEMT and the proposed H-HEMT devices. The H-HEMT shows great superiority of high breakdown voltage and low on-state resistance compared with the Conv HEMT and the A-HEMT devices. Other reported results for GaN devices are also compared as shown in Fig. 11,[25,26] and compared with other reported results the proposed H-HEMT devices also show good trade-off between BV and $R_{on,sp}$. With little sacrifice of the $R_{on,sp}$ the hybrid dielectric zone structure could effectively modulate the electric field distributions in the buffer and the GaN channel, thus the BV and FOM of the H-HEMT is significantly improved. Therefore the proposed H-HEMT shows great prospect in power electronics applications due to its high breakdown voltage and low on-state resistance.

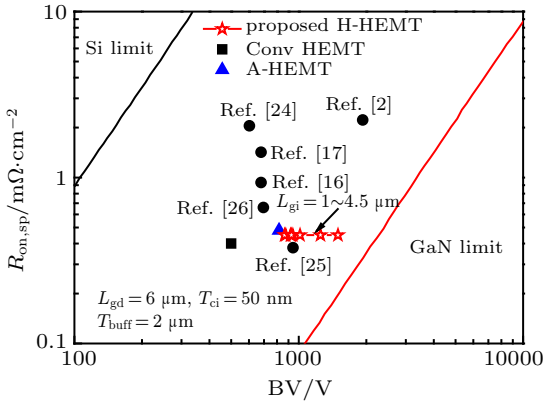


Fig. 11. Benchmarking the BV and $R_{on,sp}$ for the proposed H-HEMT devices compared with the Conv HEMT, A-HEMT and other reported results for GaN HEMTs.

3.3. The *C–V* and switching properties

The *C–V* characteristics of the three HEMTs have been simulated and the results are shown in Fig. 12. The three interelectrode capacitances C_{gs}, C_{gd} and C_{ds} are simulated, and they are converted into C_{iss}, C_{oss} and C_{rss} by[27]

$$C_{iss} = C_{gs} + C_{gd}, \quad C_{oss} = C_{gd} + C_{ds}, \quad C_{rss} = C_{gd}. \tag{2}$$

During the *C–V* simulations, gate voltage (V_{gs}) is set as 0 V and frequency f_s is set as 1 MHz. As shown in Fig. 12(a), the C_{iss} values of the Conv HEMT, the A-HEMT, and the proposed H-HEMT are 0.12 pF, 0.11 pF, 0.09 pF and 0.095 pF, respectively, at $V_{gs} = 0$ V and $V_{ds} = 400$ V. Compared with the Conv HEMT the C_{iss} of the proposed H-HEMT at $V_{ds} = 400$ V is slightly lower due to the electrons in the GaN channel depleted by the AlGaN back barrier.

Similar to C_{iss} the C_{oss} and C_{rss} of the H-HEMT are slightly lower than that for the Conv HEMT at $V_{ds} = 400$ V. Output charge Q_{oss} can be derived from the C_{oss}–V_{ds} characteristics shown in Fig. 12(b) by the integration of the C_{oss} from 0 V to 400 V, and the calculated Q_{oss} of the Conv HEMT,

the A-HEMT and the H-HEMT are 0.03 nC, 0.033 nC and 0.047 nC, respectively. The figure of merit of $R_{on}Q_{oss}$ for the H-HEMT is identified as 212 mΩ·nC, which is much lower than that of 940 mΩ·nC reported in Ref. [16]. The degree of the decrease of the C_{rss} (from 0 V to 400 V) for the proposed H-HEMT is larger than that of the Conv HEMT, which means more significant depletion zone extension for the H-HEMT, thus the proposed H-HEMT could undertake higher breakdown voltage and have higher switching speed. The *C*–*V* results indicate that the proposed H-HEMT shows great prospect in power switching applications due to its small C_{iss}, C_{oss} and $R_{on}Q_{oss}$.

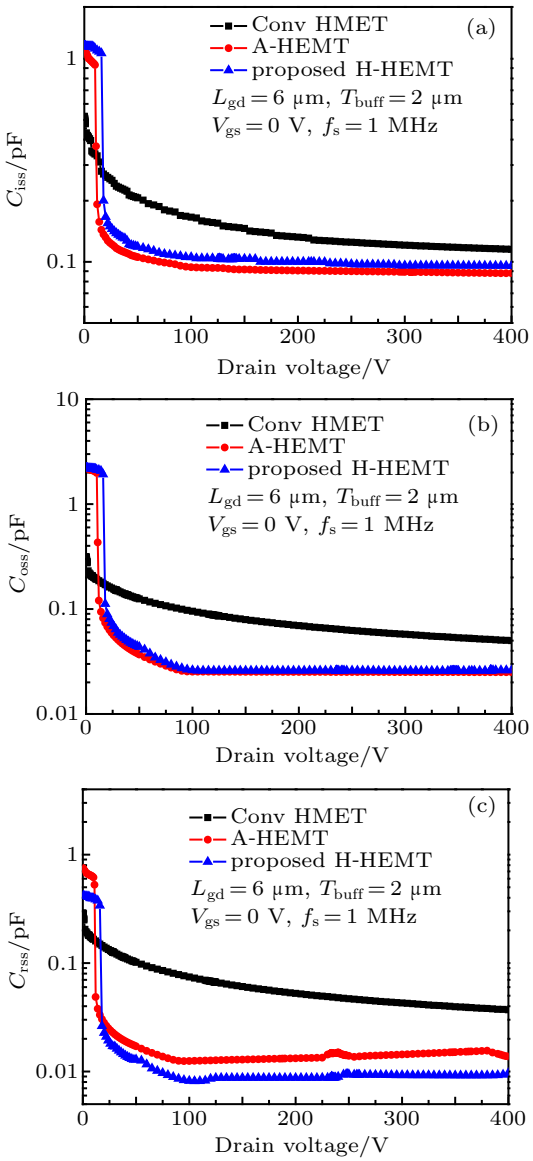


Fig. 12. Simulated *C*–*V* results of the Conv HEMT, the A-HEMT, and the proposed H-HEMT, where (a) refers to C_{iss}, (b) refers to C_{oss} and (c) refers to C_{rss}.

Based on the hybrid simulation shown in Fig. 3 the switching performances of the HEMTs have been simulated at 1 MHz switching frequency. Figure 13 shows the V_{ds}, V_{gs} and I_{ds} waveform during turn-on and turn-off processes. It can be seen that the H-HEMT has smaller turn-on time and smaller turn-off time compared with the Conv HEMT. The t_r and t_f and the switching speed dV_{ds}/dt are extracted from Fig. 13, as listed in Table 2. The Conv HEMT has t_r of 1.26 ns similar to the reported results in Ref. [16], and the t_r is reduced to as small as 0.51 ns for the proposed H-HEMT (with dV_{ds}/dt of 627 V/ns). For the H-HEMT, t_f is also significantly reduced compared with the Conv HEMT, and the dV_{ds}/dt is still as high as 87 V/ns for the H-HEMT at 1 MHz switching frequency. The calculated switching loss extracted from Fig. 13(a) for the Conv HEMT, A-HEMT and H-HEMT are 50 mW, 11 mW, and 11 mW, respectively. With optimization of L_{gi}, T_{ci} and L_{gd} the proposed H-HEMT possesses high breakdown voltage (1490 V), low $R_{on,sp}$ (0.45 mΩ·cm^2), low $R_{on}Q_{oss}$ (212 mΩ·nC), high turn-on speed (627 V/ns) and high turn-off speed (87 V/ns) at the same time, demonstrating its great prospect in power electronics applications.

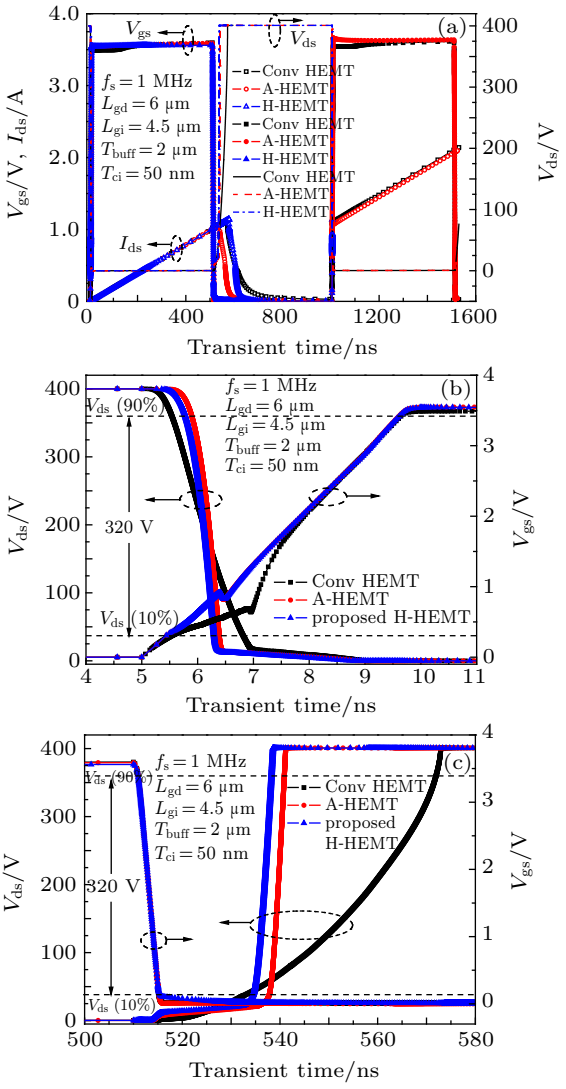


Fig. 13. Simulated turn-on waveform (a) and turn-off waveform (b) for the Conv HEMT, the A-HEMT, and the proposed H-HEMT.

Table 2. Turn-on and turn-off speeds of the GaN HEMTs.

HEMT	t_r	dV_{ds}/dt (turn-on)	t_f	dV_{ds}/dt (turn-off)
Conv HEMT	1.26 ns	254 V/ns	38.43 ns	8.33 V/ns
A-HEMT	0.49 ns	653 V/ns	3.02 ns	106 V/ns
Proposed H-HEMT	0.51 ns	627 V/ns	3.66 ns	87 V/ns
Ref. [18] (200 kHz)	1.2 ns	266 V/ns	–	–

4. Conclusions

A novel p-GaN gate GaN HEMT with AlGaN buffer and high-*k*/low-*k* hybrid dielectric zone is proposed and optimized using the Silvaco TCAD simulation tools. During the simulations the DC, breakdown, *C*–*V*, and switching properties of the proposed H-HEMT have been characterized, and the L_{gi}, T_{ci} and L_{gd} have been optimized. High breakdown voltage of 1490 V, low on-state resistance of 0.45 mΩ·cm^2 and high Baliga's figure of merit of 5.3 GW/cm^2, small $R_{on}Q_{oss}$ (212 mΩ·nC), high turn-on speed (627 V/ns@1 MHz) and high turn-off speed (87 V/ns@1 MHz) are obtained at the same time for the proposed GaN H-HEMT with L_{gd} of 6 μm, L_{gi} of 4.5 μm, T_{ci} of 50 nm. Compared with the Conv HEMT BV, turn-on speed, turn-off speed of the proposed H-HEMT is increased by 990 V, 373 V/ns, and 78 V/ns, respectively.

References

[1] Hudgins J L, Simin G S, Santi E and Khan M A 2003 *IEEE Trans. Power Electron.* **18** 907

[2] Dora Y, Chakraborty A, McCarthy L, Keller S, DenBaars S P and Mishra U K 2006 *IEEE Electron Dev. Lett.* **27** 713

[3] Wang Z X, Du L, Liu J W, Wang Y, Jiang Y, Ji S W, Dong S W, Chen W W, Tan X H, Li J L, Li X J, Zhao S L, Zhang J C and Hao Y 2020 *Chin. Phys. B* **29** 027301

[4] Liu J, Wang L Q and Huang Z X 2019 *Acta Phys. Sin.* **68** 248501 (in Chinese)

[5] Bao S Q G W, Ma X H, Chen W W, Yang L, Hou B, Zhu Q, Zhu J J and Hao Y 2019 *Chin. Phys. B* **28** 067304

[6] Uemoto Y, Hikita M, Ueno H, Matsuo H, Ishida H, Yanagihara M, Ueda T, Tanaka T and Ueda D 2006 *IEEE International Electron Devices Meeting*, San Francisco, CA, December 11–13, 2006, pp. 1–4

[7] Ueda T, Handa H, Kinosita Y, Umeda H, Ujita S, Kajitani R, Ogawa M, Tanaka K, Morita T, Tamura S, Ishida H and IshidaM 2014 *IEEE International Electron Devices Meeting*, San Francisco, CA, December 15–17, 2014, pp. 11.3.1–11.3.4

[8] Ishida M, Ueda T, Tanaka T and Ueda D 2013 *IEEE Trans. Electron Dev.* **60** 3053

[9] Huang X C, Liu Z Y, Lee F C and Li Q 2015 *IEEE Trans. Electron Dev.* **62** 270

[10] Han P C, Wu C H, Ho Y H, Yan Z Z and Chang E Y 2019 31*st IEEE International Symposium on Power Semiconductor Devices and ICs (ISPSD)* Shanghai, China, May 19–23, 2019, pp. 427–430

[11] Wu C H, Han P C, Luc Q H, Hsu C Y, Hsieh T E, Wang H C, Lin Y K, Chang P C, Lin Y C and Chang E Y 2018 *IEEE J. Electron Dev. Soc.* **6** 893

[12] Zhu M H, Ma J, Nela L, Erine C and Matioli E 2019 *IEEE Electron Dev. Lett.* **40** 1289

[13] Zhou G N, Wan Z Y, Yang G Y, Jiang Y, Sokolovskij R, Yu H and Xia G R 2020 *IEEE Trans. Electron Dev.* **67** 875

[14] Chen Y Q, Feng J T, Wang J L, Xu X B, He Z Y, Li G Y, Lei D Y, Chen Y and Huang Y 2020 *IEEE Trans. Electron Dev.* **67** 566

[15] Ge M, Cai Q, Zhang B H, Chen D J, Hu L Q, Xue J J, Lu H, Zhang R and Zheng Y D 2019 *Chin. Phys. B* **28** 107301

[16] Handa H, Ujita S, Shibata D, Kajitani R, Shiozaki N, Ogawa M, Umeda H, Tanaka K, Tamura S, Hatsuda T, Ishida M and Tetsuzo U 2016 *IEEE International Electron Devices Meeting (IEDM)* San Francisco, CA, December 3–7, 2016, pp. 10.3.1–10.3.4

[17] Tanaka K, Morita T, Umeda H, Kaneko M, Kuroda M, Ikoshi A, Yamagiwa H, Okita H, Hikita M, Yanagihara M, Uemoto Y, Takahashi S, Ueno H, Ishida H, Ishida M and Ueda T 2015 *Appl. Phys. Lett.* **107** 163502

[18] Chu R M, Hughes B, Chen M, Brown D, Li R, Khalil S, Zehnder D, Chen S, Williams A, Garrido A, Musni M and Boutros K 2013 *IEEE 71st Device Research Conference*, Notre Dame, IN, June 23–26, 2013, pp. 199–200

[19] Lee H S, Piedra D, Sun M, Gao X, Guo S P and Palacios T 2012 *IEEE Electron Dev. Lett.* **33** 982

[20] Hilt O, Knauer A, Brunner F, Treidel E B and Würfl J 2011 *IEEE 23rd International Symposium on Power Semiconductor Devives & ICs*, San Diego, CA, May 23–26, 2011, pp. 239–242

[21] Tang C J and Shi J X 2013 *Semiconduct. Sci. Technol.* **28** 115011

[22] Bai Z Y, Du J F, Liu Y, Xin Q, Liu Y and Yu Q 2017 *Solid-State Electron.* **133** 31

[23] Medjdoub F, Derluyn J, Cheng K, Leys M, Degroote S, Marcon D, Visalli D, Hove M V, Germain M and Borghs G 2010 *IEEE Electron Dev. Lett.* **31** 111

[24] Tang Z K, Jiang Q M, Lu Y Y, Huang S, Yang S, Tang X and Chen K J 2013 *IEEE Electron Dev. Lett.* **34** 1373

[25] Treidel E B, Brunner F, Hilt O, Cho E, Würfl J and Tränkle G 2010 *IEEE Trans. Electron Dev.* **57** 3050

[26] Treidel E B, Hilt O, Brunner F, Sidorov V, Würfl J and Tränkle G 2010 *IEEE Trans. Electron Dev.* **57** 1208

[27] Wang H X, Wei J, Xie R L, Liu C, Tang G F and Chen K J 2017 *IEEE Trans. Power Electron.* **32** 5539